The N-Terminal Subdomain of Insulin-like Growth Factor (IGF) Binding Protein 6. Structure and Interaction with IGFs †

ARTICLE *in* BIOCHEMISTRY · APRIL 2007

Impact Factor: 3.02 · DOI: 10.1021/bi0619876 · Source: PubMed

0888-8809/04/$15.00/0
Printed in U.S.A.

Molecular Endocrinology 18(11):2740–2750

doi: 10.1210/me.2004-0248

C-Terminal Domain of Insulin-Like Growth Factor (IGF) Binding Protein-6: Structure and Interaction with IGF-II

STEPHEN J. HEADEY, DAVID W. KEIZER, SHENGGEN YAO, GEOFFREY BRASIER, PHILLIP KANTHARIDIS, LEON A. BACH, AND RAYMOND S. NORTON

The Walter and Eliza Hall Institute of Medical Research (S.J.H., D.W.K., S.Y., R.S.N.), Parkville 3050, Australia; and Department of Medicine (S.J.H., G.B., P.K., L.A.B.), University of Melbourne, Austin Hospital, Heidelberg 3084, Australia

IGFs are important mediators of growth. IGF binding proteins (IGFBPs) 1–6 regulate IGF actions and have IGF-independent actions. The C-terminal domains of IGFBPs contribute to high-affinity IGF binding and modulation of IGF actions and confer some IGF-independent properties, but understanding how they achieve this has been constrained by the lack of a three-dimensional structure. We therefore determined the solution structure of the C-domain of IGFBP-6 using nuclear magnetic resonance (NMR). The domain consists of a thyroglobulin type 1 fold comprising an α-helix followed by a loop, a three-stranded antiparallel β-sheet incorporating a second loop, and finally a disulfide-bonded flexible third loop. The IGF-II binding site on the C-domain was identified by examining NMR spectral changes upon complex formation. It consists of a largely hydrophobic surface patch involving the α-helix, the first β-strand, and the first and second loops. The site was confirmed by mutagenesis of several residues, which resulted in decreased IGF binding affinity. The IGF-II binding site lies adjacent to surfaces likely to be involved in glycosaminoglycan binding of IGFBPs, which might explain their decreased IGF affinity when bound to glycosaminoglycans, and nuclear localization. Our structure provides a framework for understanding the roles of IGFBP C-domains in modulating IGF actions and conferring IGF-independent actions, as well as ultimately for the development of therapeutic IGF inhibitors for diseases including cancer. (*Molecular Endocrinology* 18: 2740–2750, 2004)

IGFs I AND II are widely expressed polypeptides that promote cell proliferation, differentiation, and survival by endocrine, paracrine, and autocrine mechanisms. The IGF system is the major control pathway of physiological growth in mammals (1). Aberrant regulation of the IGF system is implicated in many diseases, including cancer, diabetes, and atherosclerosis (1–3). Targeting the IGF system may therefore provide novel therapeutic opportunities for many common diseases.

IGF actions are finely regulated by a family of six high-affinity IGF binding proteins (IGFBPs 1–6) (4–6). IGFBPs inhibit IGF actions by competing with the IGF-I receptor (IGFIR) for IGF binding. They can also enhance IGF actions in some situations by mechanisms that are incompletely understood. In addition, IGF-independent actions of some IGFBPs, including inhibition of cell proliferation and survival, have been described recently (6).

IGFBP-6, the subject of the present study, differs functionally from other IGFBPs in binding IGF-II with 20- to 100-fold higher affinity than IGF-I, whereas IGFBPs 1–5 do not have a marked IGF binding preference. As a consequence, IGFBP-6 is a relatively specific inhibitor of IGF-II actions (7). Consistent with the notion that inhibiting IGF actions may decrease cancer growth, IGFBP-6 inhibits growth of IGF-II-dependent tumors *in vitro* and *in vivo* (8, 9).

IGFBPs consist of three domains of approximately equal size (4, 6). The N- and C-terminal domains are each internally disulfide-linked and share a high degree of sequence homology across the family (10). In contrast, there is little homology among their central L-domains. The disulfide linkages of the N-domain of IGFBP-6 differ from those of other IGFBPs (10), whereas the C-domain disulfides are the same in all IGFBPs so far studied (10–12). Both the N- and C-domains of IGFBPs are implicated in high-affinity IGF binding because isolated N- and C-domains bind IGFs with lower affinity than full-length IGFBPs (6).

The three-dimensional structures of full-length IGFBPs have not yet been determined. The only structural information available is for residues 40–92 of the

Abbreviations: C-BP-6, C-domain of IGFBP-6; DQF-COSY, double-quantum filtered correlation spectroscopy; HSQC, $^{15}N-^{1}H$ heteronuclear single-quantum coherence; IGFBP, IGF binding protein; IGFIR, IGF-I receptor; IGF-II/M6PR, IGF-II/mannose-6-phosphate receptor; K_d, dissociation constant; NMR, nuclear magnetic resonance; NOESY, nuclear Overhauser enhancement spectroscopy; R_2, spin-spin relaxation rate; TOCSY, total correlation spectroscopy.

***Molecular Endocrinology* is published monthly by The Endocrine Society (http://www.endo-society.org), the foremost professional society serving the endocrine community.**

N-domain of IGFBP-5, alone (13) and in complex with IGF-I (14). This region, dubbed mini-IGFBP-5, binds IGFs with 10- to 200-fold lower affinity than full-length IGFBP-5 (13). It contains a hydrophobic IGF binding site within a novel protein fold, and mutation of key hydrophobic residues within this region of IGFBP-5 and the equivalent region of IGFBP-3 dramatically reduces IGF binding, confirming its importance in IGF binding (15).

Residues in the C-domain are also important for high affinity IGF binding, as shown by deletion and site-directed mutagenesis (11, 16). However, the lack of a structure of the C-domain of any IGFBP precludes a complete understanding of the molecular mechanisms by which IGFBPs modulate IGF actions. We have therefore determined the structure of the C-domain of IGFBP-6 (C-BP-6) using NMR. In addition, we have mapped the surface of C-BP-6 that interacts with IGF-II by monitoring changes in the NMR spectrum of ^{15}N-labeled C-domain upon titration with IGF-II. The C-domain of IGFBP-6 has a thyroglobulin type 1 fold that interacts with IGF-II through a largely hydrophobic surface patch involving the α-helix, the first β-strand, and the first and second loops. This site was confirmed by site-directed mutagenesis of a number of residues, resulting in decreased IGF binding.

RESULTS

Structure of the C-Domain of IGFBP-6

The construct used in this study consisted of a 27-residue vector-encoded leader sequence followed by 80 residues from the C-terminal domain of IGFBP-6 (Gly161 to Gly240; numbering corresponds to the full-length IGFBP-6 precursor, SWISSPROT accession no P24592) (17). Residues from the leader sequence did not contain defined secondary structure and are not included in the following discussion. Parameters characterizing the final family of 20 structures of C-BP-6 and structural statistics are tabulated in Table 1, which shows that the structures fit well with experimentally derived distance and angle constraints. The structures of C-BP-6 have been deposited with the Protein Data Bank (accession no. 1RMJ) (18).

Stereo views of the final 20 structures superimposed over the backbone of residues 161–222 are shown in Fig. 1. The structure of C-BP-6 begins with a four-turn α-helix from Pro162 to Thr176, followed by the first loop, from Glu177 to Thr184. This is followed by the first strand of a three-stranded antiparallel β-sheet encompassing residues Leu185 to Asp191. The end of the first strand is stabilized by the Cys163-Cys190 disulfide bridge and the packing of relatively conserved hydrophobic side chains between the α-helix and the strand. Residues Asp191-Gly194 form a well-defined type I β-turn, which is followed by a β-bulge at Tyr196-Lys198. The protein backbone then forms the second and third strands of the β-sheet involving residues Arg199-Ser204 and Cys212-Val215, stabilized by the Cys201-Cys212 disulfide bond. A second loop spans residues Gln205-Pro211 and a second distorted type I β-turn begins at Asp216. After Pro223, there is a third, highly disordered loop, comprised largely of hydrophilic residues and restrained principally by the Cys214-Cys234 disulfide bond. The C-terminal tail, from residues Pro235-Ser240, is also disordered in the structure. A short region of well-defined structure is present in loop III from Gly230-Cys234.

Table 1. Structural Statistics for C-BP-6[a]

Nonredundant Distance Restraints	
Intra ($i = j$)	249
Sequential ($\|i - j\| = 1$)	288
Short ($1 < \|i - j\| \leq 5$)	77
Long ($\|i - j\| > 5$)	298
Dihedral Restraints	145
Hydrogen Bonds	10
Deviations from Experimental Data	
NOEs (Å)[b]	0.054 ± 0.001
Dihedrals (°)	0.41 ± 0.11
Deviations from Ideal Geometry[c]	
Bonds (Å)	0.0050 ± 0.0005
Angles (°)	0.88 ± 0.05
Impropers (°)	0.86 ± 0.10
RMSDs[d]	
All heavy atoms	1.98
Backbone heavy atoms (N, C^{α}, C′)	1.07
Ramachandran Plot[e]	
Most favored (%)	82.4
Allowed (%)	16.7
Additionally allowed (%)	0.9
Disallowed (%)	0

[a] Translational diffusion measurements (37, 38) indicated that the protein was monomeric under the solution conditions used in this study (data not shown). [b] E_{NOE} was 20.3 ± 3.3 kcal mol^{-1}, calculated using a square-well potential with force constants of 50 kcal mol^{-1} Å^2. [c] The values for the bonds, angles, and impropers show the deviations from ideal values based on perfect stereochemistry. [d] Mean pairwise RMSD (root mean square deviation) over residues 161–178, 182–205, 210–222. Mean pairwise RMSD over backbone heavy atoms of the entire C-domain was 5.08 Å. [e] As determined by the program PROCHECK-NMR for all residues present in the native sequence except Gly and Pro (49).

The angular order parameters, S, for the backbone ϕ and ψ angles and the side-chain χ^1 angles are presented in Fig. 2. The ϕ and ψ angles are well-ordered ($S_{\phi,\psi} > 0.9$) for all residues except in the three loops and the C terminus, indicating that the structure is otherwise well defined. Within the structured core of the molecule, residues in loops I and II exhibited secondary peaks in the ^{15}N-^{1}H heteronuclear single-quantum coherence (HSQC) spectrum, consistent with slow conformational exchange. The major conformation accounts for approximately 60% of the protein in solution. Pro211, located at the distal end of the second loop adopted a *cis* conformation, as defined by its C^{β} and C^{γ} chemical shifts (19), a strong Gly210

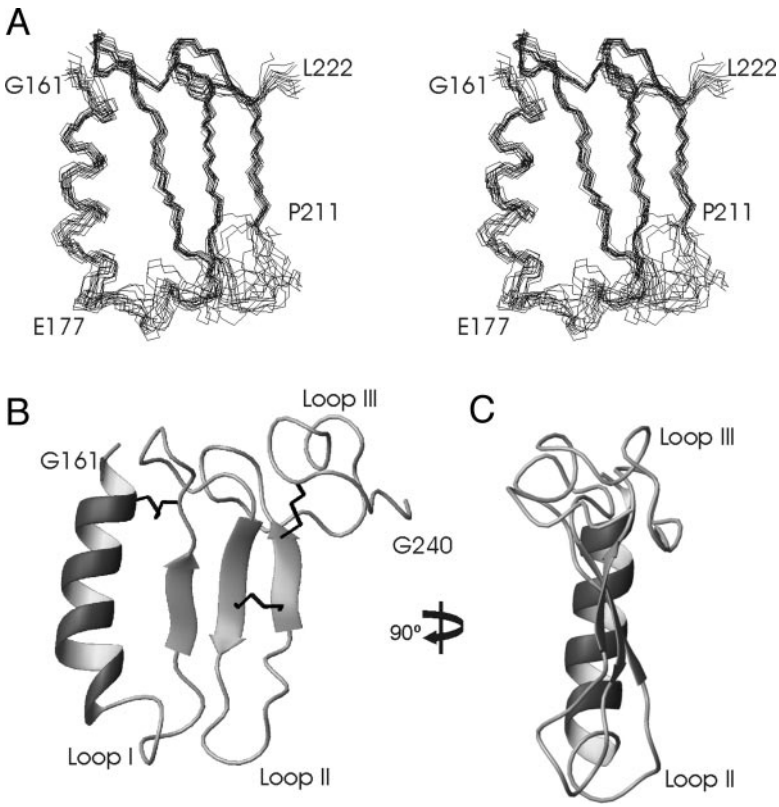

Fig. 1. C-BP-6 Structure

A, Stereo view of the family of 20 final structures, superimposed over backbone heavy (N, C^{α}, C′) atoms from Gly161 to Leu222. B, Ribbon view of the closest-to-average structure highlighting the α-helix, β-sheet, and three disulfides. C, Structure in B, rotated by 90 degrees about the vertical axis.

H^{α} to Pro211 H^{α} NOE, and the absence of Gly210 H^{α} to Pro211 H^{δ} NOEs. The *trans* form was not observed, so it is not possible to say whether *cis-trans* isomerism around the peptide bond preceding Pro211 is the source of conformational heterogeneity. All other Pro residues adopted *trans* conformations. Of the three disulfide bridges in C-BP-6, two, Cys201-Cys212 (right-handed) and Cys214-Cys234 (left-handed) are *trans* and Cys163-Cys190 (left-handed) is *cis*.

A surface representation of C-BP-6 is shown in Fig. 3. The first β-turn and the β-bulge contain a cluster of positively charged residues comprising His192, Arg193, Arg197, Lys198, and Arg199, which form part of the heparin binding domain. A surface-exposed hydrophobic patch lies between the α-helix and the first β-strand (Fig. 3A). In a DALI search (20) for structurally similar proteins, only the MHC class II-associated p41 Ii fragment, which is a cathepsin L inhibitor (PDB code 1ICF), had a similar fold (Z score 5.0). Both of these proteins adopt a thyroglobulin type 1 fold (Fig. 4).

The IGF-II Binding Site on C-BP-6

IGF-II bound C-BP-6 with a dissociation constant (K_d) in the low micromolar range, as assessed by surface plasmon resonance (21). Specific C-domain residues affected by IGF-II binding were identified from changes in ^{15}N-^{1}H HSQC spectra of ^{15}N-labeled C-BP-6 upon titration with unlabelled IGF-II. At IGF-II:C-BP-6 ratios above 0.25:1 the ^{15}N-^{1}H HSQC peaks of Thr176, Gly181, Thr184, Cys190, Ser203, Ser204, Gln205, Gly206, and Arg209 disappeared and did not reappear at IGF-II:C-domain ratios of up to 2:1, as shown in Fig. 5A. However, reducing the pH to 3.0, where binding does not occur, restored line widths in the ^{15}N-^{1}H HSQC spectrum of C-BP-6 to those observed before IGF-II addition, indicating that no irreversible changes had taken place.

The broadening of specific cross peaks in the C-BP-6 spectrum is interpreted in terms of intermediate exchange between the free and bound forms of C-BP-6, with the extent of line broadening reflecting the magnitude of the chemical shift change induced by IGF-II binding. For high-affinity interactions, with $K_d < 10^{-8}$ M, the free and bound forms are expected to be in slow exchange on the NMR time scale, and separate resonances are seen for the two forms (22, 23). For weak interactions, with K_d in the millimolar range, fast exchange is expected and cross peaks move gradually from their free to their bound frequencies upon addition of ligand. For K_d in the micromolar range, which is the case for IGF-II binding to C-BP-6, inter-

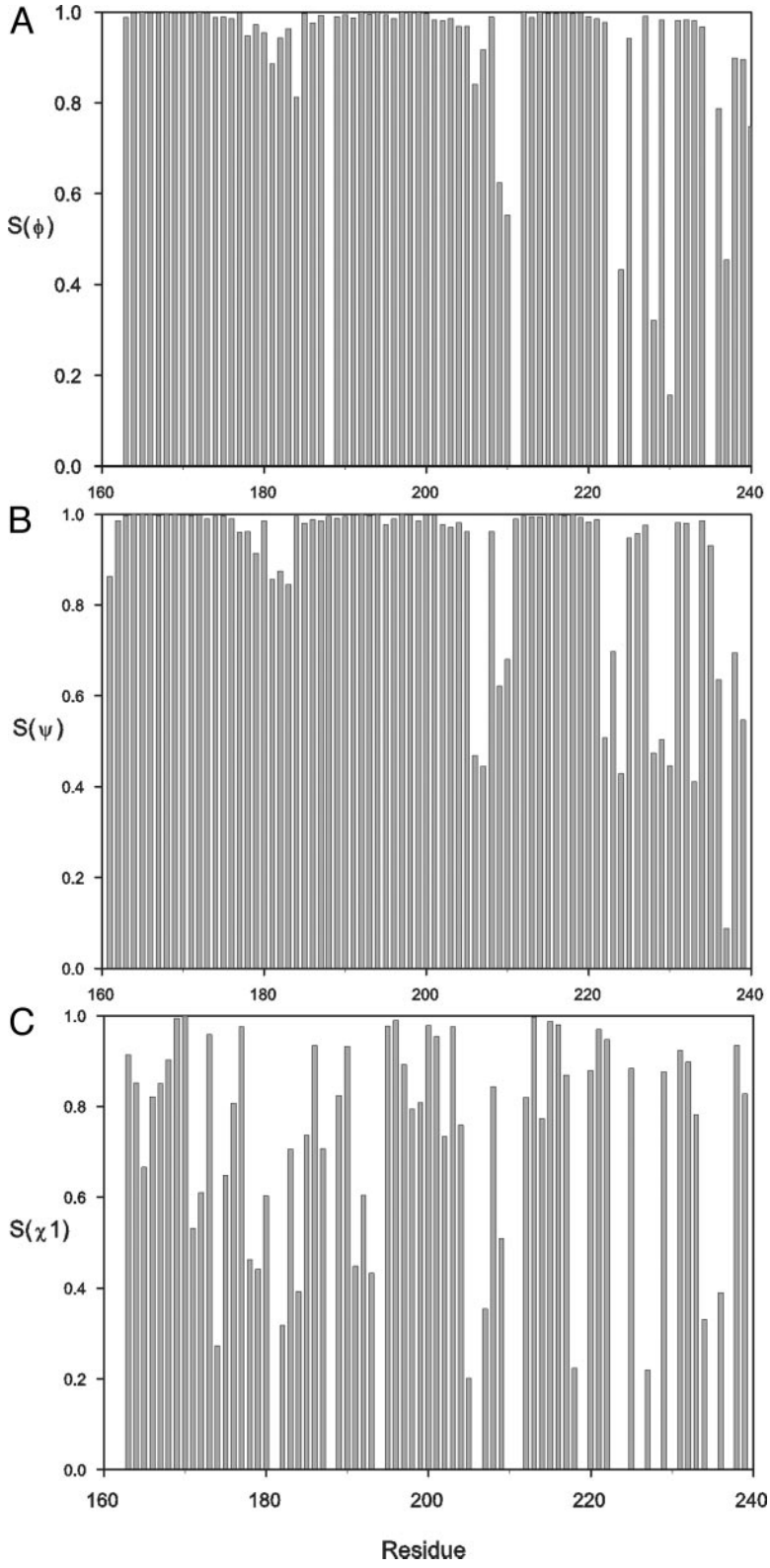

Fig. 2. Angular Order Parameters as a Function of Residue Number for C-BP-6
A, S_{ϕ}; B, S_{ψ}; and C, S_{χ_1}. Angular order parameters were calculated using MOLMOL (50).

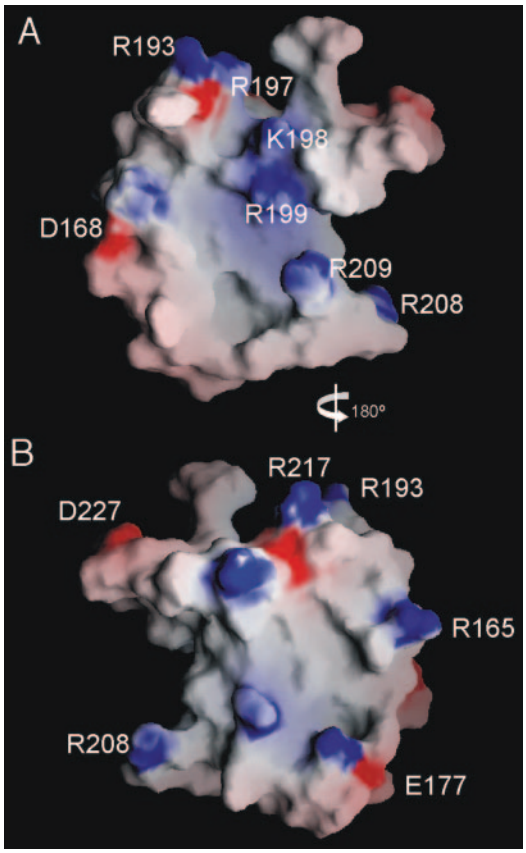

Fig. 3. Surface Representation of C-BP-6, Showing Basic Residues in *Blue* and Acidic Residues in *Red*

The two views in A and B are related by a 180-degree rotation around the vertical axis. This figure was prepared using GRASP (53).

mediate exchange is often observed, in which the exchange rates are comparable to the frequency differences between resonances from the free and bound forms. As a consequence, the affected resonances broaden upon ligand addition, and may even disappear. A few cross peaks in the spectrum of C-BP-6 shifted slightly upon IGF-II addition but remained visible (*e.g*. Arg164, Arg165, His166, and Gln175), indicating that their chemical shift perturbations in both dimensions were small enough to be in the fast exchange regime (Fig. 5A). In an attempt to alter the exchange rate regime, spectra were recorded at 5 C and 45 C at a ^{15}N-C-BP-6: IGF-II ratio of 1:1, as well as at 500 MHz. These changes, however, did not drive the exchange into the slow or fast limits. At 45 C, changes in the HSQC spectrum of C-BP-6 indicated that its conformation had begun to change.

Spin-spin relaxation rate (R_2) measurements of C-BP-6 in the presence and absence of IGF-II provided an alternative measure of spectral perturbations caused by IGF-II binding. Residues with significant increases in the relaxation rate were, in order of decreasing magnitude, Val187, Gln175, Arg165, Arg199, Gly194, Arg193, Val178, Leu174, Tyr196, Asp191, Gln200, Val215, His166, Trp213, Ala182, Leu167, Asp168, Leu171, Ser221, Cys214, and Lys198. The residues of the third loop and C-terminal tail showed no change in R_2. R_2 data from residues Asn189 and Gly210 could not be fitted due to weak signal and rapid decay for IGF-II-bound C-BP-6, whereas His192 showed rapid decay when both free and bound. Residues excluded from analysis due to peak overlap were Val170, Gln172, Gln173, Glu177, Tyr179, Arg180, Gln183, Tyr186, Arg197, Cys201, Arg202, Arg208, and Arg217.

Site-Directed Mutagenesis Confirms the IGF Binding Site of C-BP-6

Based on the above findings, Ser203, Ser204, and Gln205 were mutated to Ala and competition binding studies performed using [^{125}I]IGF-II. This mutation led to a 5-fold decrease in binding affinity for IGF-II but IGF-I affinity was not affected (Fig. 6, A and B), suggesting that these residues may be involved in the IGF-II binding preference of IGFBP-6. Asn189 is conserved in IGFBPs 1–6 and lies within the putative IGF binding site. Mutation of this amino acid to Ala resulted in 3-fold decreased binding affinity for both IGF-I and -II (Fig. 6, A and C). These results confirm that residues within the putative IGF binding site contribute to IGF binding.

Mutation of the equivalent of Gly194 in IGFBP-5 to Lys resulted in a 7-fold reduction in affinity for IGF-I (16). In contrast, mutation of this residue to Ala in IGFBP-6 had no substantial effect on IGF binding (Fig. 6, A and C).

DISCUSSION

C-BP-6 Has a Thyroglobulin Type 1 Fold

The C-domains of IGFBPs, including IGFBP-6, share sequence homology with thyroglobulin type 1 repeats (24). The MHC class II-associated p41 Ii fragment, a homolog of the thyroglobulin type 1 domain (25, 26), is the only protein with a similar fold to C-BP-6 (Fig. 4). The three disulfide pairings are conserved and the QC and CWCV motifs, along with a conserved Tyr/Phe, form the core of the molecules. Three Gly residues, two of which are in β-turns, are also conserved. Because these structurally important residues are largely conserved across the six IGFBPs, we expect the fold defined here for C-BP-6 to be found in the other five binding proteins.

Single or multiple thyroglobulin type 1 domains are found in many functionally unrelated proteins. Some of these inhibit cysteine proteases, and it has been proposed that these domains regulate proteolysis (25). The crystal structure of p41 Ii shows that its three loops are inserted into a cleft that forms the cathepsin L active site, thereby providing a mechanism of protease inhibition (25). These three loops exhibit the

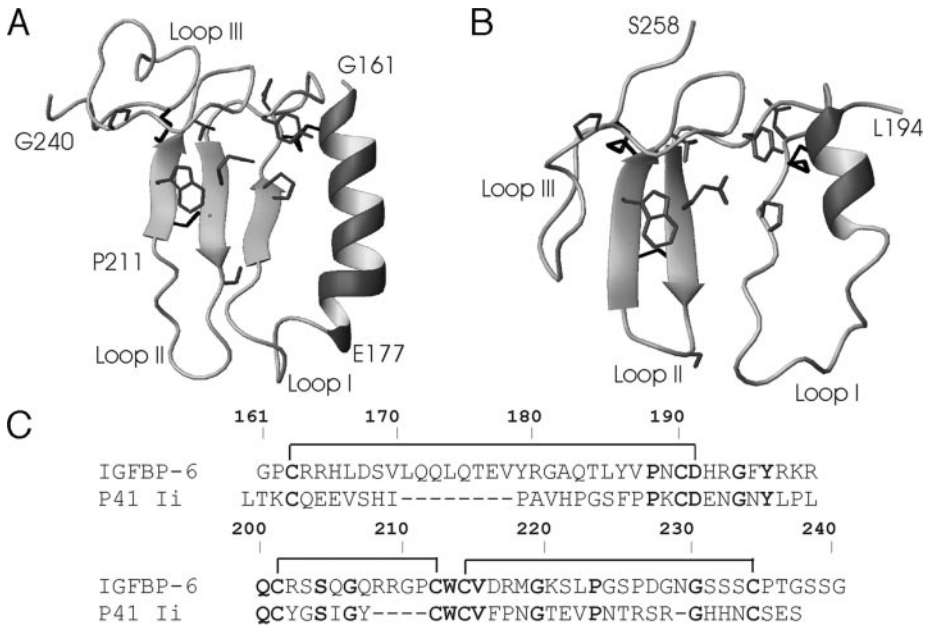

Fig. 4. Comparison of A C-BP-6 (A) with p41 Ii Fragment (B) (PDB 1ICF)

Side chains forming the conserved motifs of a thyroglobulin type 1 fold and the disulfide bonds are shown. This figure was prepared using MOLMOL (50). C, Sequence alignments of C-BP-6 and a MHC class II-associated p41 Ii fragment, which is a cathepsin L inhibitor with 28% identity. Disulfide linkages are shown as *horizontal lines* above C-BP-6 and are conserved in p41 Ii.

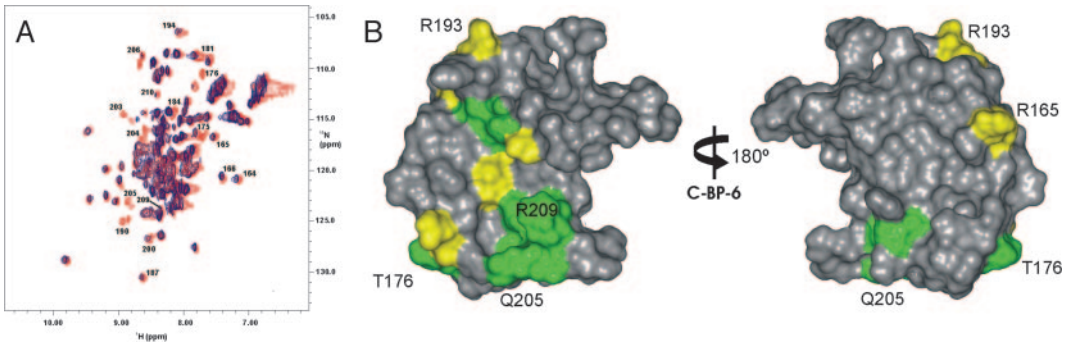

Fig. 5. IFG-II Binding Surface on C-BP-6 Identified by NMR

A, ^{1}H-^{15}N HSQC of C-BP-6 in the presence (*blue*) and absence (*red*) of IGF-II (IGF-II: C-BP-6 1.0). B, Surface of C-BP-6 showing residues whose ^{1}H-^{15}N cross peaks disappeared upon IGF-II binding in *green* and those that displayed large increases in the ^{15}N transverse relaxation rate (R_2) in *yellow*.

greatest divergence in amino acid sequence between p41 Ii and C-BP-6 and are also the most divergent among the IGFBP C-domains. Nevertheless, IGFBPs-3, -5, and -6 inhibit proteolysis of IGFBP-4 (27). This activity was isolated to a basic region of the C-domains of these IGFBPs corresponding to residues Cys190-Gln207 in C-BP-6. This region includes residues homologous with those that are important for cathepsin binding in the second loop of p41 Ii; in particular, Ser230 of p41 Ii interacts with cathepsin L residues in the catalytic site and this Ser is conserved in all IGFBPs except IGFBP-4.

The IGF-II Binding Site on C-BP-6

The IGF-II binding site on C-BP-6 is located on one face of the molecule encompassing the hydrophobic region between the α-helix and the first extended strand, the first strand itself, and the first and second loops (Fig. 5B). This surface includes residues Leu174, Val178, Gly181, Val187, Asn189, Cys190, Gly194, Arg199, Ser203, Ser204, Gln205, and Gly206. Arg164, Leu167, Leu171, Ala182, Pro188, and Cys201 are also believed to be part of the binding site but this could not be verified experimentally due to spectral complexity. In contrast to the relatively compact IGF-I binding surface of the N-domain of IGFBP-5 (13, 14), this is a larger surface and it is likely that the binding site involves the summation of a large number of relatively weak contacts between the C-domain and IGF-II. It is therefore not surprising that mutation of residues within the C-domain site results in relatively modest

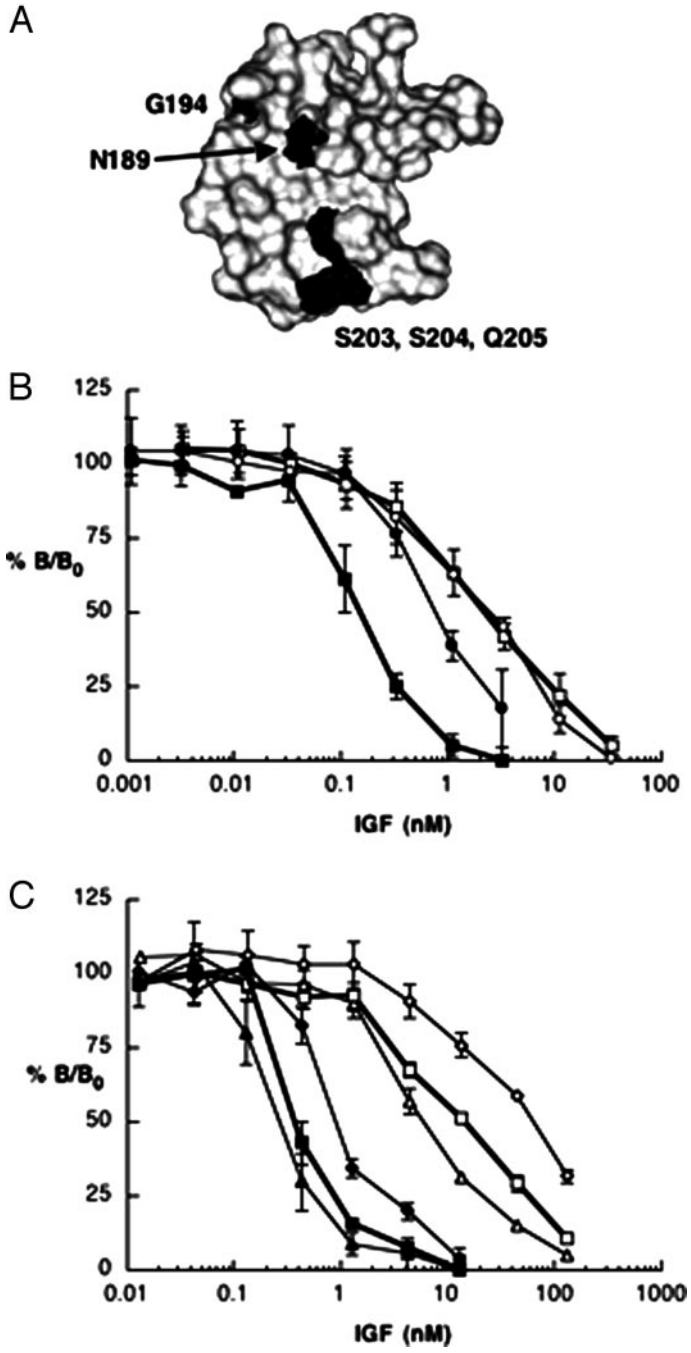

Fig. 6. Analysis of the IGF-II Binding Surface on C-BP-6 by Site-Directed Mutagenesis

A, Sites of C-BP-6 mutation. Residues were mutated to Ala and IGF binding compared with native IGFBP-6. B and C, Competitive solution binding study using [^{125}I]IGF-II and unlabeled IGF-II (*filled symbols*) or IGF-I (*open symbols*). Results are shown as the percentage of specific binding in the absence of unlabeled IGF (% B/B_0), and represent the mean ± SEM of three independent experiments. B, Binding curves of IGFBP-6 (*squares*) and [Ala203, Ala204, Ala205]IGFBP-6 (*circles*). Total specific binding (B_0) was 19.8 ± 1.9% and 13.3 ± 0.7% of total counts for IGFBP-6 and [Ala203, Ala204, Ala205]IGFBP-6, respectively. C, Binding curves of IGFBP-6 (*squares*), [Ala189]IGFBP-6 (*diamonds*), and [Ala194]IGFBP-6 (*triangles*). Total specific binding (B_0) was 26.7 ± 2.2%, 19.6 ± 1.7% and 18.5 ± 2.2% of total counts for IGFBP-6, [Ala189]IGFBP-6, and [Ala194]IGFBP-6, respectively.

reductions in IGF binding affinity. Indeed, many such mutations might be necessary to completely abolish C-domain interactions with the IGFs.

This surface is distinct from the loop regions of p41 Ii involved in cathepsin L binding, and its hydrophobic nature suggests a different mode of interaction. Thus,

although C-BP6 and p41 Ii share a common thyroglobulin type 1 fold, they use quite distinct parts of the structure to achieve their biological functions. It will be interesting to see which parts of this fold are used by yet other proteins containing this domain, such as nidogen, a basement membrane glycoprotein that binds laminin, and saxiphilin, a transferrin-like protein that binds the neurotoxin saxitoxin.

Before the present study, there was no clear consensus as to the location of the IGF binding site in the C-domain of IGFBPs. There have therefore only been limited studies of the roles of C-domain residues of IGFBPs in high-affinity IGF binding. Knowledge of the structure of C-BP-6 now allows these studies to be cohesively integrated, and they are consistent with the proposed IGF binding site. In general, they show that the region spanning the last disulfide bond of the C-domain is not substantially involved in IGF binding, consistent with the lack of ordered structure of this part of C-BP-6. Thus, point and deletion mutations in this region of the C-domains of IGFBP-1 (28), IGFBP-2 (11), and IGFBP-4 (29) did not substantially affect IGF binding. However, photoaffinity-labeled IGF-I contacted IGFBP-2 residues beyond the equivalent of Gly230 of C-BP-6 (30); it is difficult to reconcile this with our structural information, although other findings of that study are consistent with ours (as discussed in the next paragraph).

More proximal C-domain deletions have a more marked effect on IGF binding. Deletion of IGFBP-4 beyond the equivalent of Cys212 decreased IGF-I binding approximately 7-fold (29). Deletion beyond the C-BP-6 equivalent of His192 in bovine IGFBP-2 resulted in a decrease in binding affinity that was more marked for IGF-II, suggesting that His192-Gly206 are involved in IGF binding (11). This is consistent with our mutagenesis results implicating Ser203, Ser204, and Gln205 in IGF-II but not IGF-I binding; these residues appear to contribute to the IGF-II binding preference of IGFBP-6. A contact site in IGFBP-2 corresponding to Val178-His192 of C-BP-6 was identified using photoaffinity-labeled IGF-I (30), which is also consistent with the effect of mutation of Asp189 in the present study. This residue is conserved in all IGFBPs; in contrast to the Ser203, Ser204, and Gln205 mutation, both IGF-I and -II binding were affected equally by mutation of Asn189, suggesting that it is involved in IGF binding but not in IGF-II binding specificity.

Mutation in IGFBP-5 of the C-BP-6 equivalent of Gly194 to Lys decreased IGF-I binding approximately 7-fold (16, 31). In contrast, mutation of this residue to Ala in IGFBP-6 had no effect on IGF binding. Gly194 is found on the surface of C-BP-6 in the first β-turn (Figs. 1 and 6A), and its NMR peak is affected by IGF-II binding, suggesting that it forms part of the IGF binding site. However, it is a conserved residue in the thyroglobulin type 1 fold and its mutation may also have altered relationships between secondary structural elements, thereby indirectly changing the conformation of the IGF binding site. The observed decreased IGF binding affinity for IGFBP-5 may therefore have been due to substitution of a large, charged residue for a Gly, resulting in perturbation of local structure, in contrast to the more conservative mutation to Ala in IGFBP-6. Mutation of a second IGFBP-5 residue, the C-BP-6 equivalent of Gln200 to Ala, decreased IGF binding approximately 5-fold (16, 31). Although circular dichroism spectroscopy suggested that this mutation did not lead to gross conformational change (32), Gln200 is only surface exposed to a very limited extent on the opposite face of the C-domain to the IGF binding site, and the effect of its mutation is likely to be due to structural disturbance rather than direct interaction with IGFs. Interestingly, mutation of the equivalent of Gly194 to Ala in conjunction with mutation of Gln200 resulted in a larger decrease in IGF binding than mutation of either residue alone (32); this may have resulted from the combined effect of two relatively small perturbations in structure.

Other Functional Motifs on C-BP-6

C-domains of some IGFBPs interact with other biomolecules that modulate IGFBP effects on IGF actions and mediate IGF-independent effects. C-BP-6 includes a region rich in basic residues that have been implicated in binding glycosaminoglycans in IGFBP-3 and -5 (33). IGFBP-6 also binds to glycosaminoglycans, although binding is inhibited by its own O-linked glycans (34). It has been postulated that the basic-rich region of IGFBP-5 forms an α-helix, resulting in the formation of a highly charged heparin binding site (31); our C-BP-6 structure clearly shows that this is not the case.

Binding to glycosaminoglycans results in cell association and reduced IGF binding affinity; these processes contribute to potentiation of IGF activity by IGFBPs under some circumstances. In IGFBP-3 and -5, the equivalents of His192, Arg193, Arg197, and Gln205 of CBP-6 are involved in binding heparin (33), and these key residues are located on the same face of C-BP-6 (Fig. 3A). Mutation of these basic residues does not affect IGF binding by IGFBP-5 (33). However, the heparin binding patch is adjacent to the putative IGF binding site on C-BP-6, so that glycosaminoglycan binding may interfere physically with IGF binding.

IGFBPs-3 and -5 localize to the nucleus, where they interact with nuclear components including transcription factors. Nuclear localization is thought to be especially important for IGF-independent actions of these IGFBPs, and a basic sequence (Arg228, Gly229, Arg230, Lys231, and Arg232 in IGFBP-3) is essential for this process (35). The equivalent residues in C-BP-6, Gln205-Arg209, form the exposed second loop of C-BP-6 (Fig. 1), which is contiguous with the glycosaminoglycan binding site (Fig. 3). Other basic residues in the same region facilitate nuclear localization (35), and some of these are also important for heparin binding. IGFBP-6 may localize to the nucleus in some cells (36).

Conclusions

The C-BP-6 structure described here adds important information to our understanding of the structure-function relationships of IGFBPs. The distinct binding sites and modes of interaction for cathepsins and IGF-II within a common thyroglobulin type 1 fold exemplify the multifunctional nature of proteins containing this fold. The proximity of the IGF and glycosaminoglycan binding sites provides a structural basis for the decrease in IGF binding affinity after IGFBP interaction with glycosaminoglycans. The site-directed mutagenesis studies show the utility of a structure-based approach to investigating the function of the C-domain, although further studies are clearly needed to obtain a complete understanding of IGF-IGFBP interactions. Because excess IGF activity is implicated in diseases such as cancer, this knowledge provides a valuable framework for the development of high affinity therapeutic IGF antagonists.

MATERIALS AND METHODS

Samples

The expression, labeling and NMR assignment of ^{15}N- and ^{13}C-/^{15}N-labeled human IGFBP-6 C-domain have been described previously (17). Recombinant IGF-II was kindly provided by Kerrie McNeil and John Wallace (University of Adelaide, Adelaide, Australia).

NMR Spectroscopy

NMR experiments for structure determination were performed in Shigemi tubes with 1 mM protein in 95% H_2O/5% ^2H_2O containing 10 mM sodium acetate (pH 4.5) and 0.02% (wt/vol) sodium azide. Spectra were recorded mostly at 25 C on a Bruker DRX-600 spectrometer using a triple-resonance probe equipped with triple-axis gradients. Diffusion measurements were performed using a pulsed field gradient longitudinal eddy-current delay pulse sequence (37, 38). Two-dimensional DQF-COSY (double-quantum filtered correlation spectroscopy), TOCSY (total correlation spectroscopy), and NOESY (nuclear Overhauser enhancement spectroscopy) (τ_m = 150 msec) spectra were acquired using the ^{15}N-labeled sample with ^{15}N decoupling, both in H_2O and ^2H_2O. ^{15}N HSQC, HNHA, HNHB, ^{15}N-edited NOESY-HSQC (τ_m = 100 and 150 msec) and ^{15}N-edited TOCSY spectra were also acquired using the ^{15}N-labeled sample. HNCA, HNCACB, HNCO, HN(CA)CO, HCCH-TOCSY, HBHA(CO)NH and ^{13}C-edited NOESY (τ_m = 150 msec) spectra were recorded using ^{13}C, ^{15}N-labeled sample. Standard pulse sequences were used for data acquisition, and water suppression was achieved using either WATERGATE (39) or echo- and anti-echo coherence selection schemes (40). For the ^{13}C- and ^{15}N-edited NOESY spectra, a recycle delay of 1.6 sec was used, and data matrix sizes were 1024 × 92 × 144 and 2048 × 48 × 160, respectively. An additional ^{15}N-edited NOESY spectrum was acquired at 800 MHz with a mixing time of 100 msec. The ^{1}H chemical shifts were referenced to the water peak, and the ^{13}C and ^{15}N chemical shifts were referenced indirectly using the ^{13}C/^{1}H and ^{15}N/^{1}H γ-ratios (41). NMR data were processed in XWINNMR version 3.1 (Bruker Biospin) and analyzed using XEASY version 1.3 (42). ^{1}H, ^{13}C, and ^{15}N chemical shifts assignments have been deposited in the BioMagResBank database with accession no. 5545 (17).

ϕ Angle restraints were based on $^3J_{HNH\alpha}$ coupling constants derived from intensity ratios in the HNHA spectrum (43) $^3J_{HNH\alpha}$ values < 6 Hz were converted to restraints of -60 ± 30 degrees, whereas $^3J_{HNH\alpha} > 8$ Hz were restrained to -120 ± 40 degrees. For the remaining residues, the ϕ angle was restricted to the negative value if a positive ϕ could be excluded based on NOE data (44). ψ Angle restraints were determined from the intensity ratios of H^N-$H^{\alpha(i)}$/H^N-$H^{\alpha(i-1)}$ cross-peaks in the ^{15}N NOESY-HSQC spectrum and only applied to regions of well-defined secondary structure (45). ϕ and ψ angle restraints were also determined with TALOS (46). Hydrogen bond restraints were assigned based on exchange rates of ^{15}N-bound protons measured by running a series of two-dimensional ^{1}H-^{15}N HSQC spectra at 15 min, 30 min, 1 h, and 4 h after dissolving the protein in ^2H_2O at 10 C. Hydrogen bonds were only included in latter rounds of structure calculations in regions of well-defined structure that initially converged on the basis of NOE restraints alone.

NOE Assignments and Structure Calculations

NOE cross peaks were assigned and initial structures calculated using the CANDID module of CYANA (47). Input data for CANDID were the chemical shift and peak intensity lists from the ^{13}C- and ^{15}N-edited NOESY spectra, dihedral angle restraints, and disulfide bonds. The resulting structures were further refined manually using CYANA 1.0.3 torsion angle dynamics algorithm and then in Xplor-NIH (48) using the distance geometry-simulated annealing protocol. Finally, the protein was refined in a shell of water using Xplor-NIH (48) on the basis of NOE and dihedral restraints and the geometry of bonds, angles, and impropers. A final family of 20 structures was selected on the basis of stereochemistry and energy considerations and analyzed using PROCHECK-NMR (49) and MOLMOL (50). The coordinates for the IGFBP-6 C-domain have been deposited in the Protein Data Bank (18) under accession code 1RMJ.

C-Domain Interaction with IGF-II

The IGF-II binding site on C-BP-6 was defined by monitoring NMR spectral perturbations upon complex formation. Unlabeled IGF-II was titrated into 0.3 mM ^{15}N-CBP-6 in 10 mM sodium acetate, 0.02% (wt/vol) sodium azide in 95% H_2O/5% ^2H_2O at pH 4.5. A series of two-dimensional ^{15}N, ^{1}H-HSQC spectra was recorded at IGF-II:^{15}N-C-BP-6 ratios of 0.05:1, 0.10:1, 0.15:1, 0.20:1, 0.25:1, 0.5:1, 0.75:1, 1:1, 1.25:1, 1.5:1, 1.75:1, and 2:1. C-BP-6 ^{15}N transverse relaxation times (T_2) were measured at a 1:1 ratio. Fourteen relaxation delays were used, ranging from 15.4 to 308 msec with a recycle delay of 2.2 sec. The matrix size was 2048 × 180, with 32 scans per t_1 increment. R_2 for the various ^{15}N, ^{1}H resonances were compared with those obtained for unbound C-domain (51).

Site-Directed Mutagenesis of IGFBP-6

Site-directed mutagenesis was performed to confirm the putative IGF-II binding site in the C-domain of IGFBP-6. The template for mutagenesis was the cDNA for full-length IGFBP-6 inserted into pProEX-HTb (Invitrogen Life Technologies, Carlsbad, CA), which encodes an N-terminal His_6-tag with a tobacco etch virus protease site. Three mutants were made, in which Ala was substituted for 1) Ser203, Ser204, and Gln205; 2) Asn189; and 3) Gly194, respectively. Mutations were made using the QuikChange method (Stratagene, La Jolla, CA) with the following oligonucleotides:

1) CGGCAGTGCCGCGCCGCCGCGGGGCAGCGCC and GGCGCTGCCCCGCGGCGGCGCGGCACTGCCG;

2) CACTCTACGTGCCGGCTTGTGACCATCG and CGATGGTCACAAGCCGGCACGTAGAGTG;

3) TTGTGACCATCGCGCGTTCTACCGGAAGC and GCTTCCGGTAGAACGCGCGATGGTCACAA

Mutations were confirmed by DNA sequencing. Proteins, including native IGFBP-6, were expressed in *E. coli* and purified by NiNTA-agarose chromatography. After elution, proteins were incubated with His_6-tagged tobacco etch virus protease (Invitrogen Life Technologies) for 3 h at room temperature. Uncleaved protein, His_6 tags and the protease were then removed by incubation with NiNTA-agarose. Cleavage efficiency was typically 40%.

Competitive Binding Assays

Competitive binding studies was carried out as described previously (52). Native IGFBP-6 or mutants were incubated with [^{125}I]IGF-II (2×10^4 cpm, specific activity 140–180 μCi/μg) ± unlabeled IGF-II (0.0013–13.4 nM) or IGF-I (0.013–131 nM) for 18 h at 4 C in 0.1 M sodium phosphate buffer (pH 7.4) containing 0.1% BSA and 0.02% sodium azide. Free tracer was removed by incubation with ice-cold 5% charcoal, 2% BSA in Dulbecco's PBS, followed by centrifugation and counting of bound radioactivity in supernatants. Specific binding was calculated by subtracting the amount of tracer in samples without added IGFBP from total binding. Within each of three independent experiments, points were measured in duplicate; results are shown as mean ± SEM. Relative IGF binding affinities were estimated by comparing IGF concentrations at which 50% displacement of tracer occurred.

Acknowledgments

We thank Nigel Parker (Department of Medicine University of Melbourne) for help with C-BP-6 expression and purification, Kerrie McNeil and John Wallace (University of Adelaide) for generously providing IGF-II, and Wolfgang Bermel (Bruker Biospin, Karlsruhe, Germany) for recording the 800 MHz NOESY-HSQC spectrum.

Received June 18, 2004. Accepted August 4, 2004.

Address all correspondence and requests for reprints to: R. S. Norton, The Walter and Eliza Hall Institute of Medical Research, 1G Royal Parade, Parkville 3050, Australia. E-mail: ray.norton@wehi.edu.au.

This work was supported in part by Grants 114156 (to L.A.B. and R.S.N.) and 299960 (to L.A.B.) from the National Health and Medical Research Council of Australia. S.J.H. and G.B. are recipients of National Health and Medical Research Council Dora Lush Postgraduate Research Scholarships.

S.J.H. and D.W.K. contributed equally to this paper.

REFERENCES

1. Oldham S, Hafen E 2003 Insulin/IGF and target of rapamycin signaling: a TOR de force in growth control. Trends Cell Biol 13:79–85
2. Yu H, Rohan T 2000 Role of the insulin-like growth factor family in cancer development and progression. J Natl Cancer Inst 92:1472–1489
3. Bach LA 1999 The insulin-like growth factor system: basic and clinical aspects. Aust NZ J Med 29:355–361
4. Bach LA, Rechler MM 1995 Insulin-like growth factor binding proteins. Diabetes Rev 3:38–61
5. Jones JI, Clemmons DR 1995 Insulin-like growth factors and their binding proteins: biological actions. Endocr Rev 16:3–34
6. Baxter RC 2000 Insulin-like growth factor (IGF)-binding proteins: interactions with IGFs and intrinsic bioactivities. Am J Physiol Endocrinol Metab 278:E967–E976
7. Bach LA 1999 Insulin-like growth factor binding protein-6: the "forgotten" binding protein? Horm Metab Res 31:226–234
8. Grellier P, De Galle B, Babajko S 1998 Expression of insulin-like growth factor-binding protein 6 complementary DNA alters neuroblastoma cell growth. Cancer Res 58:1670–1676
9. Gallicchio MA, Kneen M, Hall C, Scott AM, Bach LA 2001 Overexpression of insulin-like growth factor binding protein-6 inhibits rhabdomyosarcoma growth in vivo. Int J Cancer 94:645–651
10. Neumann GM, Bach LA 1999 The N-terminal disulfide linkages of human insulin-like growth factor-binding protein-6 (hIGFBP-6) and hIGFBP-1 are different as determined by mass spectrometry. J Biol Chem 274:14587–14594
11. Forbes BE, Turner D, Hodge SJ, McNeil KA, Forsberg G, Wallace JC 1998 Localization of an insulin-like growth factor (IGF) binding site of bovine IGF binding protein-2 using disulfide mapping and deletion mutation analysis of the C-terminal domain. J Biol Chem 273:4647–4652
12. Chelius D, Baldwin MA, Lu X, Spencer EM 2001 Expression, purification and characterization of the structure and disulfide linkages of insulin-like growth factor binding protein-4. J Endocrinol 168:283–296
13. Kalus W, Zweckstetter M, Renner C, Sanchez Y, Georgescu J, Grol M, Demuth D, Schumacher, R, Dony C, Lang K, Holak TA 1998 Structure of the IGF-binding domain of the insulin-like growth factor-binding protein-5 (IGFBP-5): implications for IGF and IGF-I receptor interactions. EMBO J 17:6558–6572
14. Zesławski W, Beisel HG, Kamionka M, Kalus W, Engh RA, Huber R, Lang K, Holak TA 2001 The interaction of insulin-like growth factor-I with the N-terminal domain of IGFBP-5. EMBO J 20:3638–3644
15. Imai Y, Moralez A, Andag U, Clarke JB, Busby Jr WH, Clemmons DR 2000 Substitutions for hydrophobic amino acids in the N-terminal domains of IGFBP-3 and -5 markedly reduce IGF-I binding and alter their biologic actions. J Biol Chem 275:18188–18194
16. Bramani S, Song H, Beattie J, Tonner E, Flint DJ, Allan GJ 1999 Amino acids within the extracellular matrix (ECM) binding region (201–218) of rat insulin-like growth factor binding protein (IGFBP)-5 are important determinants in binding IGF-I. J Mol Endocrinol 23:117–123
17. Headey SJ, Yao S, Parker NJ, Kantharidis P, Bach LA, Norton RS 2003 ^{1}H, ^{13}C and ^{15}N resonance assignments of the C-terminal domain of insulin-like growth factor binding protein-6 (IGFBP-6). J Biomol NMR 25:251–252
18. Berman HM, Battistuz T, Bhat TN, Bluhm WF, Bourne PE, Burkhardt K, Feng Z, Gilliland GL, Lype L, Jain S. Fagan P, Marvin J, Padilla D, Ravichandran V, Schneider B, Thanki N, Weissig H, Westbrook JD, Zardecki C 2002 The Protein Data Bank. Acta Crystallogr D Biol Crystallogr 58:899–907
19. Schubert M, Labudde D, Oschkinat H, Schmieder P 2002 A software tool for the prediction of Xaa-Pro peptide bond conformations in proteins based on ^{13}C chemical shift statistics. J Biomol NMR 24:149–154
20. Holm L, Sander C 1993 Protein structure comparison by alignment of distance matrices. J Mol Biol 233:123–138
21. Headey SJ, Leeding KS, Norton RS, Bach LA, Contributions of the N- and C-terminal domains of insulin-like growth factor (IGF) binding protein-6 to IGF binding. J Mol Endocrinol, in press
22. Meyer B, Peters T 2003 NMR spectroscopy techniques for screening and identifying ligand binding to protein receptors. Angew Chem Int Ed Engl 42:864–890
23. Zuiderweg ER 2002 Mapping protein-protein interactions in solution by NMR spectroscopy. Biochemistry 41:1–7

24. Kiefer MC, Masiarz FR, Bauer DM, Zapf J 1991 Identification and molecular cloning of two new 30-kDa insulin-like growth factor binding proteins isolated from adult human serum. J Biol Chem 266:9043–9049
25. Gunčar G, Pungerčič G, Klemenčič I, Turk V, Turk D 1999 Crystal structure of MHC class II-associated p41 Ii fragment bound to cathepsin L reveals the structural basis for differentiation between cathepsins L and S. EMBO J 18:793–803
26. Chiva C, Barthe P, Codina A, Gairi M, Molina F, Granier C, Pugniere M, Inui T, Nishio H, Nishiuchi Y, Kimura T, Sakakibara S, Albericio F, Giralt E 2003 Synthesis and NMR structure of p41icf, a potent inhibitor of human cathepsin L. J Am Chem Soc 125:1508–1517
27. Fowlkes JL, Thrailkill KM, George-Nascimento C, Rosenberg CK, Serra DM 1997 Heparin-binding, highly basic regions within the thyroglobulin type-1 repeat of insulin-like growth factor (IGF)-binding proteins (IGFBPs) -3, -5, and -6 inhibit IGFBP-4 degradation. Endocrinology 138: 2280–2285
28. Brinkman A, Kortleve DJ, Zwarthoff EC, Drop SL 1991 Mutations in the C-terminal part of insulin-like growth factor (IGF)-binding protein-1 result in dimer formation and loss of IGF binding capacity. Mol Endocrinol 5:987–994
29. Qin X, Strong DD, Baylink DJ, Mohan S 1998 Structure-function analysis of the human insulin-like growth factor binding protein-4. J Biol Chem 273:23509–23516
30. Horney MJ, Evangelista CA, Rosenzweig SA 2001 Synthesis and characterization of insulin-like growth factor (IGF)-1 photoprobes selective for the IGF-binding proteins (IGFBPS). Photoaffinity labeling of the IGF-binding domain on IGFBP-2. J Biol Chem 276:2880–2889
31. Song H, Beattie J, Campbell IW, Allan GJ 2000 Overlap of IGF- and heparin-binding sites in rat IGF-binding protein-5. J Mol Endocrinol 24:43–51
32. Shand JH, Beattie J, Song H, Phillips K, Kelly SM, Flint DJ, Allan GJ 2003 Specific amino acid substitutions determine the differential contribution of the N- and C-terminal domains of insulin-like growth factor (IGF)-binding protein-5 in binding IGF-I. J Biol Chem 278: 17859–17866
33. Arai T, Clarke J, Parker A, Busby Jr W, Nam T, Clemmons DR 1996 Substitution of specific amino acids in insulin-like growth factor (IGF) binding protein 5 alters heparin binding and its change in affinity for IGF-I response to heparin. J Biol Chem 271:6099–6106
34. Marinaro JA, Neumann GM, Russo VC, Leeding KS, Bach LA 2000 O-glycosylation of insulin-like growth factor (IGF) binding protein-6 maintains high IGF-II binding affinity by decreasing binding to glycosaminoglycans and susceptibility to proteolysis. Eur J Biochem 267: 5378–5386
35. Schedlich LJ, Le Page SL, Firth SM, Briggs LJ, Jans DA, Baxter RC 2000 Nuclear import of insulin-like growth factor-binding protein-3 and -5 is mediated by the importin β subunit. J Biol Chem 275:23462–23470
36. Strong DD, Chen ST, Linkhart TA, Yan T, Baylink DJ, Mohan S, IGF-binding protein-6 markedly inhibits osteoblast differentiation: evidence for an intracrine mechanism involving nuclear localization utilizing a novel nuclear localization sequence. Program of the 84th Annual Meeting of The Endocrine Society, San Francisco, CA, 2002, p 102 (Abstract OR28-4)
37. Gibbs SJ, Johnson CS 1991 A PFG NMR experiment for accurate diffusion and flow studies in the presence of eddy currents. J Magn Reson 93:395–402
38. Yao S, Howlett GJ, Norton RS 2000 Peptide self-association in aqueous trifluoroethanol monitored by pulsed field gradient NMR diffusion measurements. J Biomol NMR 16:109–119
39. Sklenar V, Piotto M, Leppik R, Saudek V 1993 Gradient-tailored water suppression for 1H–15N HSQC experiments optimized to retain full sensitivity. J Magn Reson 102:241–245
40. Tolman JR, Chung J, Prestegard JH 1992 Pure-phase heteronuclear multiplequantum spectroscopy using field gradient selection. J Magn Reson 98:462–467
41. Wishart DS, Bigam CG, Yao J, Abildgaard F, Dyson HJ, Oldfield E, Markley JL, Sykes, BD 1995 ^{1}H, ^{13}C and ^{15}N chemical shift referencing in biomolecular NMR. J Biomol NMR 6:135–140
42. Bartels C, Xia TH, Billeter M, Güntert P, Wüthrich K 1995 The program XEASY for computer-supported NMR spectral-analysis of biological macromolecules. J Biomol NMR 6:1–10
43. Kuboniwa H, Grzesiek S, Delaglio F, Bax A 1994 Measurement of HN-H α J couplings in calcium-free calmodulin using new 2D and 3D water-flip-back methods. J Biomol NMR 4:871–878
44. Ludvigsen S, Poulsen FM 1992 Positive θ-angles in proteins by nuclear magnetic resonance spectroscopy. J Biomol NMR 2:227–233
45. Gagné SM, Tsuda S, Li MX, Chandra M, Smillie LB, Sykes BD 1994 Quantification of the calcium-induced secondary structural changes in the regulatory domain of troponin-C. Protein Sci 3:1961–1974
46. Cornilescu G, Delaglio F, Bax A 1999 Protein backbone angle restraints from searching a database for chemical shift and sequence homology. J Biomol NMR 13: 289–302
47. Herrmann T, Güntert P, Wüthrich K 2002 Protein NMR structure determination with automated NOE assignment using the new software CANDID and the torsion angle dynamics algorithm DYANA. J Mol Biol 319:209–227
48. Schwieters CD, Kuszewski JJ, Tjandra N, Clore GM 2003 The Xplor-NIH NMR molecular structure determination package. J Magn Reson 160:65–73
49. Laskowski RA, Rullmannn JA, MacArthur MW, Kaptein R, Thornton JM 1996 AQUA and PROCHECK-NMR: programs for checking the quality of protein structures solved by NMR. J Biomol NMR 8:477–486
50. Koradi R, Billeter M, Wüthrich K 1996 MOLMOL: a program for display and analysis of macromolecular structures. J Mol Graph 14:51–55
51. Yao S, Headey SJ, Keizer DW, Bach LA, Norton RS 2004 C-terminal domain of insulin-like growth factor (IGF) binding protein 6: conformational exchange and correlation with IGF-II binding. Biochemistry 43:1187–1195
52. Bach LA, Hsieh S, Sakano K, Fujiwara H, Perdue JF, Rechler MM 1993 Binding of mutants of human insulin-like growth factor II to insulin-like growth factor binding proteins 1–6. J Biol Chem 268:9246–9254
53. Nicholls A, Sharp KA, Honig B 1991 Protein folding and association: insights from the interfacial and thermodynamic properties of hydrocarbons. Proteins 11:281–296

Molecular Endocrinology **is published monthly by The Endocrine Society (http://www.endo-society.org), the foremost professional society serving the endocrine community.**